Polymer 191 (2020) 122282

Contents lists available at ScienceDirect

Polymer

journal homepage: http://www.elsevier.com/locate/polymer

Isothermal step thickening in a long-spaced aliphatic polyester

Stephanie F. Marxsen [a], Manuel Häußler [b], Stefan Mecking [b], Rufina G. Alamo [a,*]

[a] FAMU-FSU College of Engineering, Department of Chemical and Biomedical Engineering, 2525 Pottsdamer St, Tallahassee, FL, 32310-6046, USA
[b] Department of Chemistry, University of Konstanz, Universitätsstraße 10, 78457, Konstanz, Germany

ARTICLE INFO

Keywords:
Crystallization
Isothermal thickening
Aliphatic polyester

ABSTRACT

Discontinuous lamellar thickening has been found at the isothermal crystallization temperatures of a long-spaced aliphatic polyester (PE-48,48) synthesized via polycondensation of the diol and diacid. The isothermal step thickening is characterized by a discrete increase in melting temperature with increasing crystallization time and an increase in heat of fusion of the high melting peak at the expense of the low melting peak. The increase in crystal thickness, quantified by SAXS, is consistent with a straightening of the chains at the basal surfaces of the lamellae to complete a full repeat of the crystalline layer. The increase in thickness and decrease in surface energy are associated with the sudden increase in crystal melting. The isothermal thickening follows a logarithmic dependence of time with a rate that increases with temperature. The thickening process is thermally activated and follows Arrhenius behavior with an activation energy of 238 ± 4 kJ/mol.

1. Introduction

Isothermal crystal thickening refers to an increase of lamellae thickness observed during isothermal crystallization. Likewise, an increase of lamellae thickness is often found on annealing polymer crystallites at a temperature higher than the temperature at which the crystals were formed but below their melting point. Here, focus is given to the isothermal crystal thickening feature.

Most polymer crystals undergo a continuous thickening process during isothermal melt-crystallization. Experimental evidence is provided mainly by small-angle X-ray scattering (SAXS) and by a shift of the longitudinal acoustic mode in Raman spectroscopy (LAM). Increases in long spacing and core lamellae thickness with time have been observed during the primary and secondary crystallization stages [1,2]. Extensive studies on linear polyethylene point to a logarithmic time dependence of the crystal thickness, especially after most of the crystallinity is developed [1–9]. Coupled with the logarithmic increase of crystal thickness, the lamellar thickness distribution extracted from LAM [4], or measured by transmission electron microscopy [10], broadens substantially, hence indicating complex thickening mechanisms. Suggested mechanisms include molecular diffusion along the chain axis of the crystal [3,11–13], an increase of the crystalline order at the crystal-amorphous interface, or at the lamellar basal surface [14], and partial melt-recrystallization [15–17].

Contrasting the continuous logarithmic time-dependence found in high molecular weight polymers, long-chain *n*-alkanes and low molecular weight fractions of polyethylene oxide (PEO) display step thickening during isothermal crystallization. These low molecular weight, monodisperse systems undergo chain folding such that crystals form with a thickness equal to an integer fraction of the full length of the chain. This quantization of chain folding originates from the rejection of chain ends to the surface of the lamellae. Upon isothermal crystallization, long-chain *n*-alkanes and low molecular weight fractions of PEO initially form crystals with a small integer number of chain folds *n*, which depends on both the crystallization temperature and the total length of the chain. Over time at the same isothermal crystallization temperature, the chains unfold to have $n-1$ folds, then $n-2$ folds, etc. until the chain is fully extended and $n = 0$. Thus, there is a transformation which occurs isothermally over time from folded to more extended chains [15,18–23]. The observed quantification of chain folding has been explained as a drive to maximize the pairing of chain ends at the surface of the lamellae [15,22]. The thermodynamic driving force for such unique refolding is viewed as a minimization of the surface free energy of folded crystals with stem length close to an integer number of the chain length. Hence, *n*-alkanes may increase or reduce their thickness in order to achieve a more thermodynamically stable structure [18,20].

The step change in crystal thickness translates to a discrete increase in the melting of the system undergoing such isothermal step thickening, which can be easily quantified by differential scanning calorimetry

* Corresponding author.
E-mail address: alamo@eng.fsu.edu (R.G. Alamo).

https://doi.org/10.1016/j.polymer.2020.122282
Received 3 January 2020; Received in revised form 9 February 2020; Accepted 11 February 2020
Available online 14 February 2020

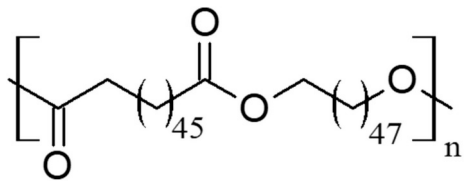

Fig. 1. Chemical repeating unit of PE-48,48.

(DSC) [15,20,21], or by *in-situ* SAXS, or AFM [18,22,24,25]. The rate of isothermal thickening was shown to increase with crystallization temperature [15,21]. Two mechanisms have been proposed to explain the discontinuous isothermal thickening of *n*-alkanes, a solid-solid chain diffusion [18,26], a melting-recrystallization process aided by thermal fluctuations [15,23], or a combination of both [27].

Fractions of PEO in a molecular weight range of 2000–7000 Da follow an integer folding crystallization, and isothermal refolding behavior analogous to the behavior of long-chain *n*-alkanes. Early studies by Spegt and Skoulios demonstrated that the crystal thickness doubled or tripled with a small change in crystallization temperature [28,29]. The observed thickness corresponded to twice, once-folded, or to the chain-extended PEO structure [30–33]. It was also later demonstrated that the initial structure that develops is a non-integer folded crystal that with time evolves isothermally to a more (thickens) or to a less (thins) extended one in stems lengths close to integer numbers of the chain length [27,33–38].

For higher molecular weight polymers, the concentration of chain ends is low; therefore, the drive to form integrally folded structures due to pairing of chain ends is basically absent. Additionally, higher molecular weight, polydisperse polymers have more chain entanglements than the oligomeric, monodisperse fractions discussed above, reducing molecular mobility and preventing consistent adjacent reentry of chains during crystallization. These factors reduce the level of crystallinity and increase the number of defects in the fold surface and crystal structure. Integral unfolding of chains leading to quantized increases in crystal thickness is therefore made virtually impossible in high molecular weight, polydisperse systems. For this reason, polymer crystals evolve toward more thermodynamically stable structures by a continuous slow thickening process, leading to a continuous increase of the crystal thickness and melting temperature. This has been well documented for many polymers, including linear polyethylene [1–10]. However, the addition of functional groups placed at a precise equal distance along the polyethylene backbone could lead to step changes in crystal thickness. Such step thickness may be found in layered crystallites of precision polyethylenes if, during crystallization, completion of a full repeating unit along the chain axis of the crystal further stabilizes the crystallite. In other words, the role of pairing of chain ends leading to more stable crystal structures in *n*-alkanes and low molar mass polymer fractions is taken over by the crystalline layer that forms by staggering the moiety or the functional group in most precision polyethylenes [39–47].

Features very similar to those observed in *n*-alkanes, such as step changes in melting and in crystal thickness during isothermal crystallization, have been observed during the crystallization of a novel, long-spaced aliphatic polyester. The thermodynamic driving force for step isothermal thickening in long-spaced polyesters is perceived to be one that minimizes the surface free energy of the crystals by staggering the ester moieties at the surface layer. The experimental data are presented in this work and are discussed on the basis of isothermal step thickening.

2. Experimental part

The polymer investigated in this work, PE-48,48, is a long-spaced aliphatic polyester of the $A_2 + B_2$ polycondensation type with 48 carbon atoms in both the diacid and diol components of its repeating unit. The chemical repeating unit of PE-48,48 is shown in Fig. 1. PE-48,48 was synthesized using a chain doubling technique, wherein monounsaturated fatty acids were converted to ultra-long (C_{48}) aliphatic α,ω-difunctional building blocks which were further polymerized. The sample used here has a number average molecular weight (M_n) of 13.6 kg/mol and a polydispersity ($Đ = M_w/M_n$) of 1.9. Details of the synthesis and molecular mass characterization were reported previously [48]. For the purposes of this work, we will consider PE-48,48 to be a pseudo-precision polyethylene, since the ester groups have alternating orientation and the number of methylene groups between each consecutive ester group alternates between 46 and 48.

2.1. Thermal analysis

Thermal behavior of PE-48,48 was obtained in a TA Q2000 differential scanning calorimeter (DSC) connected to a refrigerated RC900 cooling system to attain temperature control at sub-ambient conditions. The DSC was calibrated with indium and operated under nitrogen gas flow. To prepare the sample, the initial powder was pressed at 150 °C between two sheets of Teflon into a film of ~200 μm thickness. About 4 mg of this film was cut and encapsulated in an aluminum DSC pan. Thermal history was removed by melting in the DSC at 10 °C/min to 150 °C and holding for 5 min. To analyze the melting behavior at different heating rates, the sample was cooled from the melt at 10 °C/min to 0 °C, held for 5 min, and then heated at rates of 1, 2, 5, 10, 20, 40, and 80 °C/min. For analysis of the isothermal crystallization behavior, the sample was quenched from the melt at 40 °C/min to the desired isothermal crystallization temperature (T_c), held for the desired crystallization time (t_c), and finally heated at 10 °C/min to 150 °C to observe the melting endotherm.

2.2. Simultaneous WAXD/SAXS

Simultaneous wide-angle X-ray diffraction (WAXD) and small-angle X-ray scattering (SAXS) patterns were collected at room temperature using a Bruker Nanostar diffractometer with Incoatec microfocus X-ray source (IμS). The diffractometer was equipped with a HiStar 2D Multiwire SAXS detector and Fuji Photo Film image plate for WAXD detection. The WAXD plate was read using a Fuji FLA-7000 scanner. The incident X-ray beam was a Cu Kα line with a wavelength λ of 1.5418 Å. Samples were prepared for WAXD and SAXS by isothermal crystallization in the DSC, followed by fast quenching at 40 °C/min to room temperature.

An estimation of the level of crystallinity (X_c) was obtained from the WAXD diffractograms by the ratio of the area of the crystalline reflections over the entire area (taken as the sum of the area of the crystalline reflections and the area of the amorphous halo) as shown in Equation (1). The amorphous halo was obtained using peak fitting procedures assuming a two-phase system.

$$X_c = \frac{A_c}{A_c + A_a} \tag{1}$$

The Lorentz-corrected (Iq^2 vs q where q is the scattering vector and is related to the scattering angle 2θ by $q = 4\pi sin\theta/\lambda$) SAXS pattern and the normalized one-dimensional linear correlation function (γ) were used to estimate the long period (L) and the crystal thickness (l_c) of PE-48,48 at various T_c and t_c. γ was applied to the first order peak, and obtained as a function of the correlation distance, r, according to Refs. [49,50]:

$$\gamma(r) = \frac{\int_0^\infty I(q)q^2 \cos(rq)dq}{\int_0^\infty I(q)q^2 dq} \tag{2}$$

As it is impossible to record experimental data over the entire range of the integrals, appropriate extrapolations at each end of the data are required. Here, we used the method described in detail by Goderis et al. [51] For low q values, a second order polynomial was used to extrapolate the data to $q = 0$. At the other end of the data, the extrapolation is of

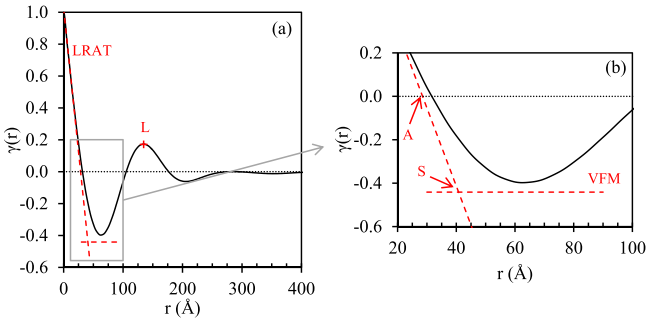

Fig. 2. (a) Example of the $\gamma(r)$ analysis for a sample of PE-48,48 that was quenched from the melt to 0 °C. LRAT is the linear regression of the autocorrelation triangle (represented by the dashed red line) and L is the long period. (b) Blown up region of the grey box in (a): shows the value of the flat minimum (VFM), the intersection of LRAT with $\gamma = 0$ (A), and the short correlation distance (S).

greater significance, since the high values of q amplify changes in extrapolated intensity. In this so-called Porod region, the following equation was used to extrapolate the data to 0 at $q \rightarrow \infty$:

$$\lim_{q\to\infty} I(q) = B(s) + \frac{K}{q^4}\exp\left(-4\pi^2\sigma^2 q^2\right) \tag{3}$$

In Equation (3), $B(s)$ is a background term, usually taken as a constant, K is the Porod constant, and σ is representative of the transition layer thickness. With appropriate extrapolations at each end of the data, Equation (2) was applied to the entire range of $I(q)$ to obtain $\gamma(r)$.

An example of $\gamma(r)$ obtained from the SAXS pattern of PE-48,48 quenched from the melt to 0 °C is shown in Fig. 2. L is directly obtained from $\gamma(r)$ as the value of r at the first maximum, indicated by the red plus sign in Fig. 2(a). The other correlation distance S, shown in the magnified correlation triangle of Fig. 2(b), is assigned to either the amorphous thickness l_a or crystal thickness l_c depending on the crystallinity. The value of S always represents the shorter distance, meaning that if the crystallinity is >50%, as for the samples studied in this work, this correlation distance would be assigned to l_a. Then, l_c can be calculated as the difference between L and l_a. In an ideal linear stacks model with sharp interfaces, the first minimum of $\gamma(r)$ intercepts the correlation triangle at S. However, for polymer crystals S is usually not available from a direct point of $\gamma(r)$, rather this value was estimated using the linear regression of the autocorrelation triangle (LRAT) to determine the linear crystallinity (φ), a method which has been described in detail previously [51–53], and is briefly outlined next.

The LRAT is shown in Fig. 2(a) as the dashed diagonal red line which follows $\gamma(r)$ closely in the low r region. The point at which the LRAT crosses $\gamma = 0$ is denoted A, as depicted in Fig. 2(b). The value of A is related to φ by the following quadratic equation:

$$\varphi^2 - \varphi + \frac{A}{L} = 0 \tag{4}$$

Solving Equation (4) leads to two possible values for φ, the one < 0.5 was used, since this value represents the short correlation distance (the solution with a value > 0.5 is then equal to $1 - \varphi$). Next, the value of the flat minimum (VFM) shown in Fig. 2 was estimated using φ:

$$VFM = \frac{-\varphi}{1-\varphi} \tag{5}$$

For all the results presented in this work, the VFM was quite close to or just below the actual first minimum of $\gamma(r)$. In Fig. 2(b), S is shown as the intersection of the LRAT with the VFM. Alternatively, the value of S can be taken as the product of φ and L. These two calculations give essentially equivalent results, which is expected and is a convenient way to verify the consistency of the analysis. Values of S presented herein were determined by taking the product of φ and L.

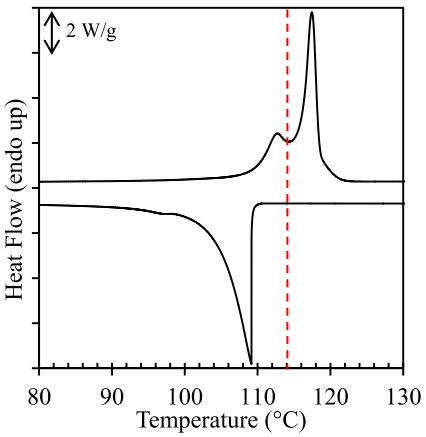

Fig. 3. Cooling exotherm and subsequent melting endotherm for PE-48,48 obtained at 10 °C/min. A dashed, red vertical line is drawn to distinguish the first and second melting peaks. (For interpretation of the references to colour in this figure legend, the reader is referred to the Web version of this article.)

3. Results and discussion

3.1. Melting behavior

The cooling exotherm and subsequent melting endotherm of PE-48,48 obtained at 10 °C/min are shown in Fig. 3. The thermograms show a relatively sharp single exotherm with a peak crystallization temperature of 108.8 °C and heat of crystallization ΔH_c of 179 J/g, and a double melting with peak temperatures of 112.7 and 117.8 °C and a total heat of fusion ΔH_m of 180 J/g. The appearance of multiple melting endotherms with only a single crystallization exotherm has generally been explained in three different ways: 1) melting-recrystallization-melting, 2) the presence of polymorphism, and 3) the melting of crystals with the same crystallographic packing but different thicknesses. To determine which of these three possibilities can explain the observed double melting endotherm of PE-48,48, further thermal studies, along with WAXD and SAXS experiments are discussed.

Melting a rapidly quenched or isothermally crystallized polymer using DSC at different heating rates is a technique commonly used to verify whether the presence of two endothermic peaks is due to melting-recrystallization-melting on heating. If such a mechanism is present, the area of the higher temperature melting peak will decrease and eventually disappear with higher heating rates, as the ability of the polymer to reorganize upon heating is diminished due to the reduced time spent near its melting temperature. In Fig. 4(a), melting endotherms recorded (after cooling from the melt at 10 °C/min to 0 °C) at various heating rates and normalized to 10 °C/min are shown. At all heating rates, the height of the low-melting peak remains basically unchanged, while the high-melting peak becomes lower as the heating rate is increased. For low heating rates, the second melting peak is sharp, and is followed by a dip below the baseline heat flow. This dip is likely the result of thermal lag.

The change in melting peak intensities after quenching to 0 °C with increasing heating rate is quantified in Fig. 4(c) as the ratio of the height of the second melting peak to the first (h_2/h_1). The height is used rather than the area for this calculation for simplicity since both give equivalent trends. With increasing heating rate, there is a steady reduction in the height of the second peak relative to the first, indicating that there is indeed a melting-recrystallization-melting mechanism at play when PE-48,48 is crystallized by dynamic cooling. The second peak never fully disappears, meaning that either a heating rate of 80 °C/min is not sufficient to eliminate the recrystallization process completely or a mixture of two populations of crystals is formed during the dynamic cooling. In the latter case, the population of less stable crystallites will be more

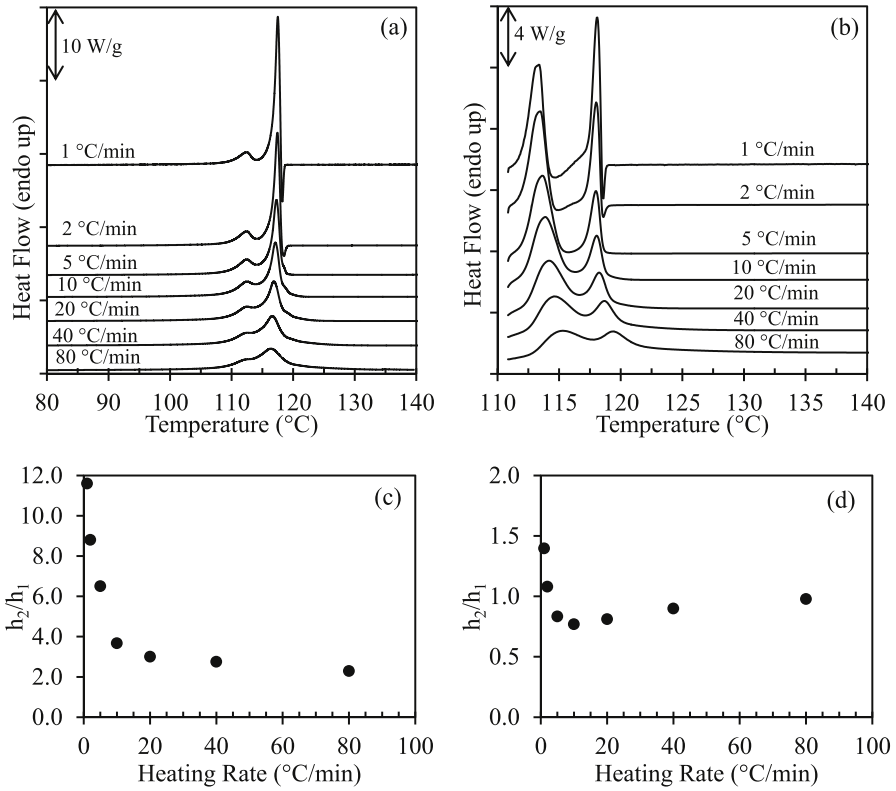

Fig. 4. Melting endotherms of PE-48,48 obtained at different heating rates after (a) cooling to 0 °C at 10 °C/min and (b) isothermal crystallization at 111 °C for 10 min. All endotherms have been normalized to the thermogram at 10 °C/min and shifted vertically for clarity. (c) Ratio of the peak heights in (a). (d) Ratio of peak heights in (b).

prone to melt-recrystallization than the more stable population of crystallites.

Interestingly, when PE-48,48 is crystallized isothermally at 111 °C, the result is different, as shown in Fig. 4(b). For heating rates of 1 and 2 °C/min, there is a clear recrystallization exotherm, indicating that melting-recrystallization-melting does occur at these low heating rates. This is confirmed quantitatively by the decrease in relative height of the high-melting peak which occurs for heating rates between 1 and 5 °C/min, as shown in Fig. 4(d). However, the recrystallization exotherm apparently disappears at a heating rate of 5 °C/min, and the relative height of the second peak stops decreasing at 10 °C/min. This result indicates that when PE-48,48 is isothermally crystallized, two populations of crystallites evolve, and heating rate of 10 °C/min is sufficient to eliminate recrystallization upon heating. The nature of the double population of crystals will be discussed later in this work. For all further melting after isothermal crystallization experiments reported here, the heating rate used is 10 °C/min.

Since isothermal crystallization leads to crystals which only recrystallize upon melting at very slow heating rates, it seems likely that upon a faster dynamic crystallization from the melt, PE-48,48 forms a "disordered" phase which is more prone to recrystallization upon heating, as mentioned. Indeed, the formation of metastable structures that melt and recrystallize on heating toward more ordered phases is a feature encountered in precision polyethylenes [39,40,54]. Depending on the depth of quenching, different metastable phases were observed recently in a work by Zhang et al. on long-spaced polyacetals [39]. Since we basically bypass the melting-recrystallization-melting process by heating at 10 °C/min after isothermally crystallizing PE-48,48, yet we still see two melting endotherms on heating, our interest now lies with the crystal structure of PE-48,48, to understand whether the difference between the two endotherms of Fig. 4(b) is due to different polymorphic structures with different thermal stabilities, or is related to the lamellar thickness.

3.2. Crystal structure

Fig. 5(a) and (b) display diffractograms of PE-48,48 fast quenched to 0 °C and isothermally crystallized at $T_c \geq 111$ °C, respectively. For a direct comparison, the diffractogram of a fast cooled linear polyethylene fraction with $M_w = 38$ kg/mol and $Đ = 1.07$ obtained in the same instrument is added to Fig. 5(b). The inset in Fig. 5(a) shows the peak deconvolution used to estimate the degree of crystallinity following a two-phase model and according to Equation (1). Clearly, there is no change in the unit cell at crystallization temperatures below and above the low melting endotherm of Fig. 3. The WAXD patterns are equivalent to the orthorhombic pattern of linear polyethylene with the (110) and (200) plane reflections at 2θ about 21.3° and 23.6°, respectively. Orthorhombic packing has been found in other asymmetric long-spaced polyesters [55,56]. Given that a nearly *all-trans* conformation appears to be the most stable when molecules consist of long polymethylene sequences, the *all-trans* orthorhombic packing is expected for PE-48,48. Moreover, as listed in Table SI1, the accommodation of the ester group in the crystalline structure expands slightly the *a* and *b* axes of the lattice with respect to the polyethylene values.

SAXS patterns recorded simultaneously to the WAXD diffractograms are displayed in Fig. 5(c) and (d). As shown, there are large differences in long-range periodicity between the crystalline structure of fast quenched PE-48,48 (Fig. 5(c)) and the structure that develops under isothermal crystallization conditions (Fig. 5(d)). The major difference is a layered crystalline structure in the latter as indicated by the prominent reflection at $q \sim 0.13$ Å^{-1} that corresponds to a spacing of 48 Å. This is the expected periodicity for the *all-trans* crystalline sequences in the lamellae of the PE-48,48 chain, accounting for a ~38° chain tilt with respect to the layer normal.

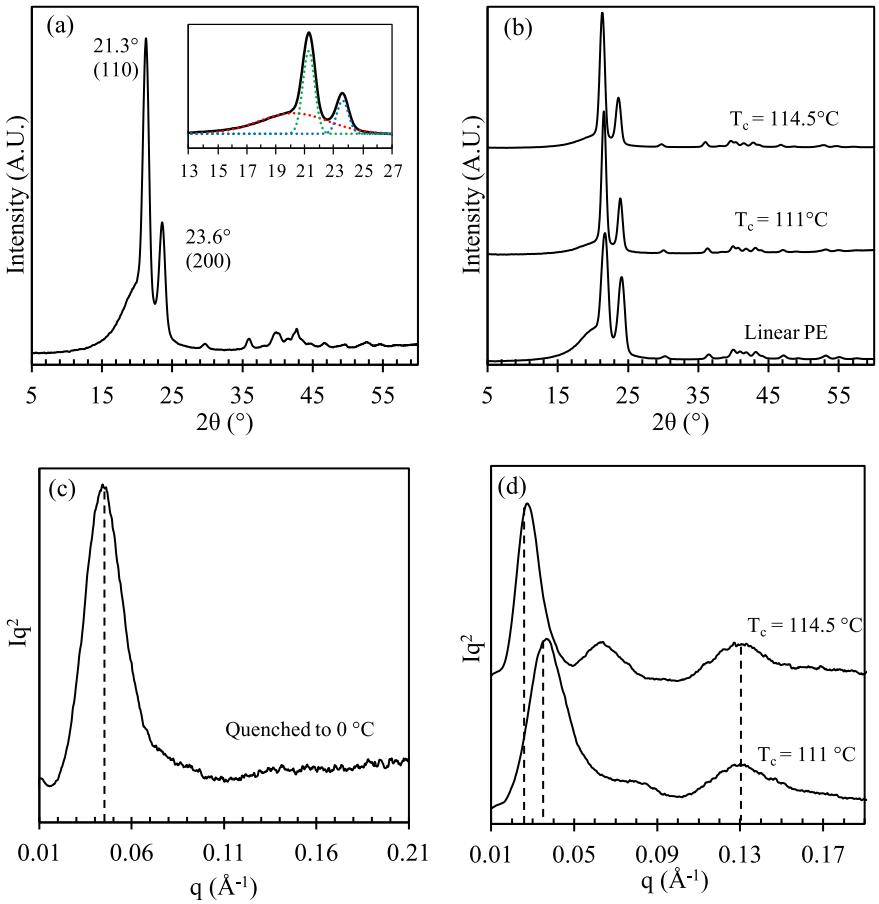

Fig. 5. Room temperature WAXD diffractograms ((a) and (b)) and Lorentz-corrected SAXS patterns ((c) and (d)) for PE-48,48 after: (a), (c) quenching from the melt to 0 °C, (the inset of (a) shows the peak deconvolution of the WAXD pattern with the amorphous halo) and (b), (d) isothermal crystallization at the indicated T_c followed by quenching to room temperature. The data have been vertically shifted for clarity.

The crystalline layer reflection is absent in the SAXS pattern of the specimen rapidly quenched to 0 °C (Fig. 5(c)). This feature confirms that a more disordered structure assembles at low temperatures. Although there are no differences in orthorhombic packing at the most fundamental level of the unit cell between fast quenched and isothermally crystallized PE-48,48 samples, the inter- and intra-molecular staggering of ester groups in the crystalline lamellae is lost under fast quenching conditions. Hence, it appears that with increasing crystallization temperature, the drive to stagger methylene sequences in the lamellae along the chain axis increases. The low angle scattering peak corresponds to the long period, which increases with increasing T_c as expected. The long period increases from ~140 Å for the quenched sample, to ~170 Å when T_c is 111 °C, and to nearly 230 Å when T_c is 114.5 °C. Furthermore, for $T_c > 111$ °C, the symmetry of the lamellae stack periodicity increases as indicated by the appearance of the second order reflection of the long spacing.

The SAXS data of Fig. 5 provide evidence for the formation of two populations of crystallites under dynamic cooling, as mentioned when discussing the data of Figs. 3 and 4. A population of layered crystallites develops quickly when reaching T_c ~110 °C, as indicated in the exotherm of Fig. 3, and a second population of un-layered crystals likely develops on further cooling at temperatures approaching 0 °C. The more disordered, un-layered structure is more prone to re-organization on heating. By the same token, layered lamellar crystallites may reorganize on slow heating to those with a higher degree of symmetry (Fig. 4(b)).

3.3. Time dependent isothermal crystallization

To better understand the source and evolution of the prominent double melting observed under isothermal crystallization, more detailed time-dependent studies were carried out. Representative melting thermograms of PE-48,48 isothermally crystallized in a large interval of temperatures covering temperatures below and above the transition between the observed double melting (~113 °C), and for increasing crystallization time, are shown in Fig. 6(a) – (d). Notably, while double endotherms result from melting crystallites formed below ~113 °C, the melting behavior for $T_c > 113$ °C is single. Hence, 113 °C is a transition crystallization temperature for the formation of a double ($T_c \leq 113$ °C) or single ($T_c > 113$ °C) population of crystallites.

In Fig. 6(a) and (b), melting endotherms recorded after isothermal crystallization at 111 and 112 °C (below the transition temperature), respectively, are shown for times (t_c) ranging from 2 to 1000 min. For short t_c, there is a single melting peak, with a peak melting temperature of around 114 °C. As t_c increases, a second, higher temperature melting peak begins to develop, which has a peak melting temperature of about 118 °C. For simplicity, we define here the first peak as LT (low temperature) and the second peak as HT (high temperature). It is apparent in these figures that as the area of HT increases, the area of LT decreases. Hence, there is an isothermal transformation from a low melting population of crystallites to a higher melting one basically within a conserved crystal system. This unique discontinuous melting behavior during crystallization resembles closely the DSC melting features associated with isothermal step thickening of folded to extended chain structures found in *n*-alkanes and low molecular weight fractions of

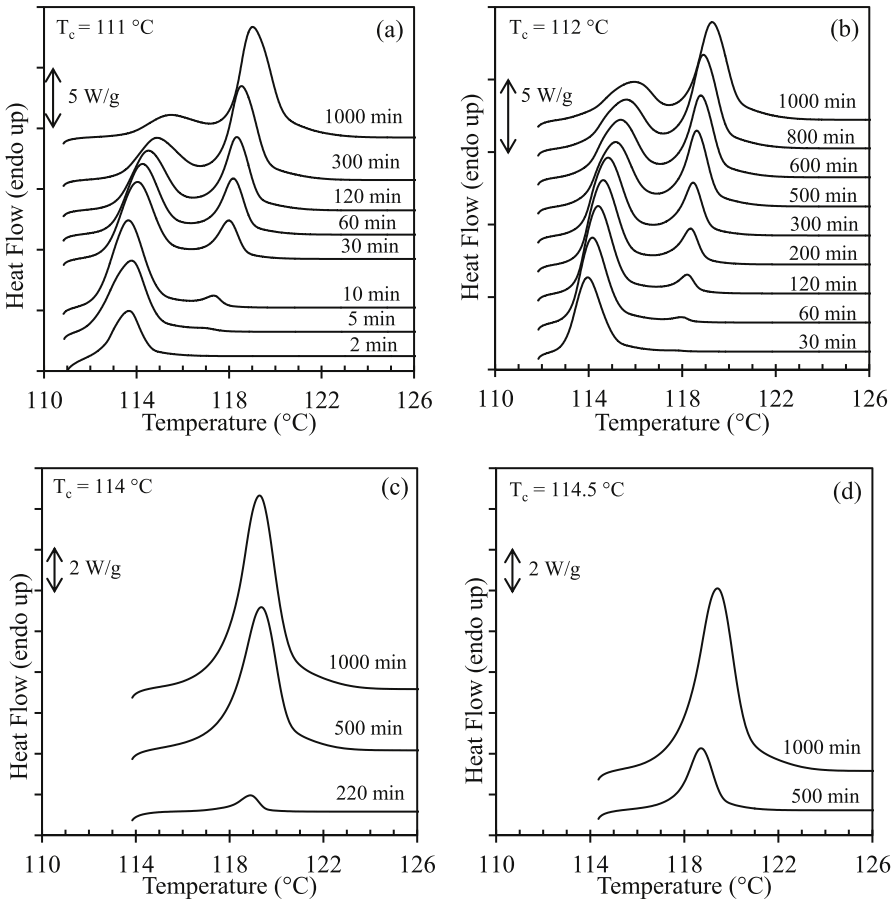

Fig. 6. Melting endotherms after isothermal crystallization for the indicated t_c for T_c of (a) 111 °C, (b) 112 °C, (c) 114 °C and (d) 114.5 °C. The endotherms have been vertically shifted for clarity.

polyethylene oxide (PEO) [15,21,33–37]. For those low molar mass systems, the isothermal step thickening is accompanied by a discrete increase in the melting temperature, a reduction in the area of the low melting peak, and an increase in the area of the high melting peak, just like what is observed here for PE-48,48. Thus, it is likely that the discontinuous change in melting of Fig. 6(a) and (b) is also due to a step increase in crystal thickness.

As will be shown later, a two-fold increase in crystal thickness is not observed here. Therefore, a possible step thickening of PE-48,48 crystals that may explain the discontinuous change in melting in Fig. 6(a) and (b) is a temporal straightening of methylene segments in the crystal-amorphous interface, or those leaving the crystalline basal surface, in order to complete an additional ester layer. As mentioned, a thicker crystal and a reduced surface tension by the complete registry of the ester layer will lead to the observed discontinuous melting.

It is important to point out that the observed changes in melting with increasing crystallization time are not artifacts from degradation or from lack of sample stability during crystallization at high temperatures, or after melting multiple times. Repeated crystallizations for the shortest times after the longest crystallization experiments, gave identical results. Furthermore, the observed double melting is not due to fractionation by molecular weight during crystallization. Since the

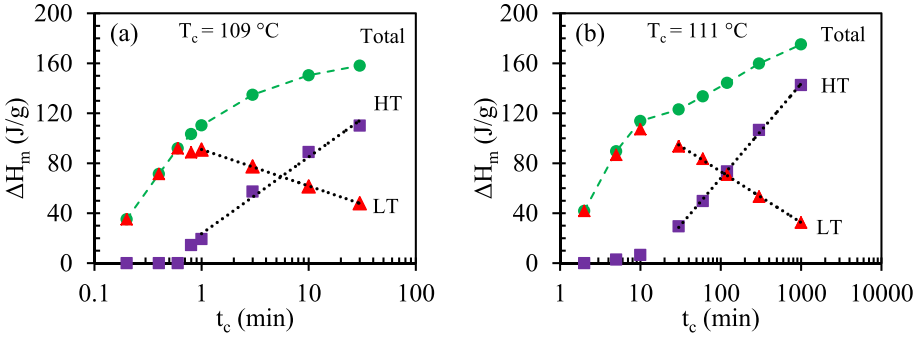

Fig. 7. Total heat of fusion (green circles), heat of fusion of the low temperature (LT) peak (red triangles), and heat of fusion of the high temperature (HT) peak (purple squares) after isothermal crystallization at (a) 109 °C and (b) 111 °C as a function of logarithm of t_c. Dashed black lines are drawn to highlight the linear temporal dependence of LT and HT with t_c. (For interpretation of the references to colour in this figure legend, the reader is referred to the Web version of this article.)

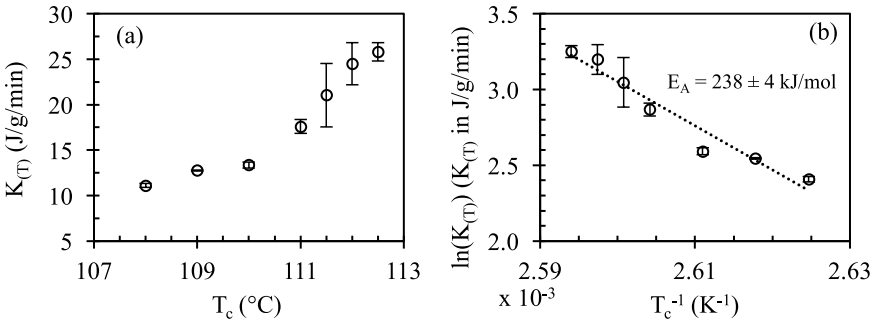

Fig. 8. (a) Rate of apparent isothermal step thickening ($K_{(T)}$) of PE-48,48 as a function of T_c. $K_{(T)}$ is taken as the slope of the linear decrease of ΔH_m of LT as a function of the logarithm of t_c. (b) Arrhenius plot of $K_{(T)}$ as a function of T_c.

polydispersity of PE-48,48 is 1.9, one could argue that above a certain temperature, the low molecular weight fraction would not crystallize, and thus we would observe only the higher temperature melting peak, as is the case here. However, if fractionation were the cause of the double melting endotherm in PE-48,48, the higher molecular weight fraction (high melting temperature) would crystallize first. Then, we would expect the high temperature melting peak to appear first, and the area of the low melting peak to increase with time, while the opposite is observed. We conclude, therefore, that fractionation cannot be the cause of the double melting endotherm in PE-48,48.

At $T_c \geq 114$ °C, above the transition temperature, only the more symmetric HT crystal structure develops. Hence, only the high temperature single melting peak is observed independent of crystallization time as shown in Fig. 6(c) and (d). In Fig. 6(c), a melting endotherm after a shorter t_c (220 min) when very few crystals have formed is shown to demonstrate that LT does not ever form at 114 °C (for tested t_c below 220 min, there is no melting peak at all).

As mentioned in the previous paragraph, for T_c below the transition temperature, HT develops at the expense of LT; this is shown quantitatively in Fig. 7 by the reduction in the area of the LT peak and the simultaneous increase of the HT peak over time. Such a result indicates a transformation from one type of crystals to a second which occurs isothermally as a function of time. This transformation is not a polymorphic one, as evidenced by WAXD diffractograms collected at room temperature after isothermal crystallization at T_c below the transition temperature for increasing time (see Figure SI1 for examples at a T_c of 111 °C). The WAXD pattern is unchanged regardless of t_c. Except for the increase in birefringence during transformation, polarized optical microscopy indicates that the transformation is not accompanied by any obvious changes in morphology, as shown in Figure SI2 for a sample crystallized isothermally at 111 °C for increasing t_c. The morphology also does not change for HT crystals formed above the transition temperature (see Figure SI3). A lack of change in the morphology and unit cell structure is expected if the difference between the two types of crystals is the lamellar thickness and the structure of the basal lamellar surface as posited earlier.

3.4. Kinetics of isothermal step thickening

Based on results presented in the prior section, we have concluded that isothermal thickening occurs in PE-48,48 in a quantized manner as a function of time for T_c below ~113 °C. Analogous to the *n*-alkanes [15,21], the isothermal transformation is quantified by the change in heat of fusion (ΔH_m) as a function of time for temperatures at which the transformation occurs. In Fig. 7, the total ΔH_m, ΔH_m of LT, and ΔH_m of HT are plotted against the logarithm of t_c for T_c of 109 (a) and 111 °C (b), which are representative of T_c below the transition temperature. After an initial increase, ΔH_m of LT decreases linearly with the logarithm of t_c. ΔH_m of HT is initially zero and starts to increase, also linearly with log t_c, at the time when LT starts to decrease.

From the logarithmic dependence of the transformation ($\Delta H_{m(t)} = \Delta H_{mo} - K_{(T)} ln(t)$), the rate constant of the isothermal step thickening ($K_{(T)}$) was obtained from the slope of the decrease of the area of the LT peak in plots analogous to those of Fig. 7. The isothermal T_c sampled ranged from 108 to 112.5 °C. The DSC was unable to achieve fast enough cooling to crystallize isothermally below 108 °C, while above 112.5 °C (near the transition temperature between 113 and 114 °C) crystallization itself was too slow to achieve a reliable linear decrease in the ΔH_m of LT. $K_{(T)}$ is plotted as a function of T_c within the abovementioned range in Fig. 8(a). It is evident that $K_{(T)}$ increases with increasing T_c. This result is consistent with what has been found for isothermal step thickening of the long-chain *n*-alkanes and low molecular weight fractions of PEO [15,27]. $K_{(T)}$ has an Arrhenius dependence on T_c, as demonstrated in Fig. 8 (b), indicating that the isothermal step thickening of PE-48,48 is a thermally activated process with an activation energy of 238 ± 4 kJ/mol.

The kinetics of isothermal thickening of a PEO fraction with M_n = 5000 g/mol were extracted from the evolution of SAXS data with time collected with a synchrotron source [27]. The formation of extended crystals at the expense of the once folded crystallites was found to follow first order kinetics and was explained as a combined effect of chain diffusion and partial melting followed by recrystallization. The rate constant also followed Arrhenius behavior with activation energy of 224.4 ± 22.4 kJ/mol. In spite of the different rate law dependence, the activation energy of the isothermal step thickening of PE-48,48 and PEO are remarkably similar. Moreover, the rate constant of the isothermal thickening of *n*-alkanes was associated with the inverse of the time at which ΔH_m of the low melting peak extrapolated to zero, i.e. the time at which full transformation was achieved [15,21]. Upon treating the *n*-alkane data with the Arrhenius equation, much higher activation energies are obtained for *n*-alkanes (400–600 kJ/mol). Hence, it appears that tighter hairpin folds in the *n*-alkane crystals require a higher activation energy barrier, and possibly partial melting as suggested, for their isothermal transformation to a more stable structure [15]. Conversely, the initial non-integer folded crystals of PEO [33,34], or those of PE-48, 48 with naturally more disorder at the basal lamellar surface, should facilitate thickening, explaining the lower activation energy values.

3.5. Long period and crystal thickness

Our interest now lies with investigation of the core crystal thickness (l_c) to confirm that the isothermal transformation of PE-48,48 observed by DSC corresponds with the expected increase in thickness. If a change in thickness does occur, we expect to see a change in SAXS patterns collected for samples isothermally crystallized at T_c below the transition temperature for increasing t_c, while no change should happen for T_c above the transition temperature. Ideally, the SAXS patterns should be collected with increasing time at the isothermal crystallization temperature. However, the long times for the observed transformation made

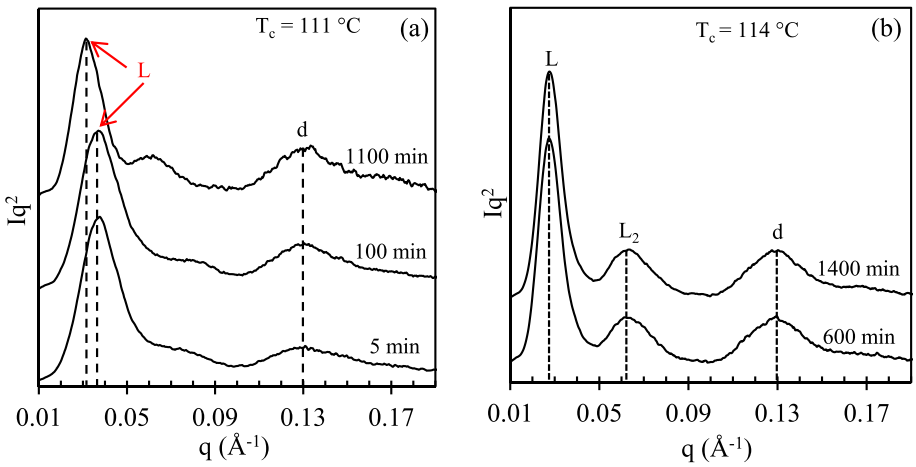

Fig. 9. Room temperature, Lorentz-corrected SAXS profiles for T_c of (a) 111 °C and (b) 114 °C for the indicated t_c. The plots have been normalized by their maximum intensity and shifted vertically for clarity.

in-situ experiments impractical. Thus, SAXS patterns were collected at room temperature after isothermal crystallization for various t_c followed by quenching at 40 °C/min to room temperature. To minimize the effect of quenching on lamellar periodicity, times were chosen after relatively high degrees of crystallinity are developed. Representative Lorentz-corrected SAXS patterns for T_c of 111 and 114 °C are shown in Fig. 9 (a) and (b), respectively.

At a T_c of 111 °C (below the transition temperature), for the relatively low values of t_c of 5 and 100 min, we observe a peak at q of ~0.037 Å^{-1}, corresponding to a long spacing (L) of ~170 Å, as shown in Fig. 9(a). For the longest t_c of 1100 min, the peak shifts to a lower value of q at ~0.032 Å^{-1} corresponding to an L of ~200 Å. Similar results were obtained for T_c of 112 and 113 °C (see Figure SI4(a)–(b)). Thus, there is indeed an increase in L as a function of t_c at T_c below the transition temperature; in the case of 111 °C, this increase is ~30 Å.

Based on the DSC analysis from the previous section, we expect no change in the SAXS pattern as a function of time at a high T_c of 114 °C. Indeed, for both t_c shown (600 and 1400 min), the SAXS patterns are essentially identical, with a peak at q of ~0.028 Å^{-1}, corresponding to an L of ~220 Å. The same invariance of L with crystallization time was found for T_c of 114.5 and 115 °C (see Figure SI4(c) and (d)).

Besides the shift to lower q of the long spacing with increasing crystallization time for $T_c \leq 113$ °C, of interest is the appearance of the second order periodicity at q ~0.06 Å^{-1} in all SAXS patterns at $T_c > 113$ °C and for $T_c \leq 113$ °C but only when the isothermal thickening is almost completed. The development of periodic order already points to a transition of the initial crystal structure toward more symmetric lamellar stacks during isothermal thickening.

All SAXS patterns display the crystalline layer peak at q ~0.131 ± 0.002 Å^{-1} which is unchanged with T_c or t_c, thus indicating the presence of layered crystals prior to and after isothermal thickening. The layer distance corresponding to the observed q is 48.0 ± 0.6 Å. If, as predicted, the PE-48,48 molecule crystallizes with an *all-trans* conformation, the theoretical expected length between consecutive ester groups can be calculated with C–C and C–O bond lengths of 1.54 and 1.43 Å respectively, and C–C–C and C–O–C bond angles of 109.5°. The calculated length is 60.9 Å. The difference gives a chain tilt of 38 ± 1° with respect to the layer normal. Similar chain tilts have been found in polyethylenes [57,58], *n*-alkanes [59] and most precision polyethylenes investigated [40,41,44]. The SAXS structural data related to the ester layer distance are tabulated for all T_c in Table SI2.

Values for the core crystal thickness, l_c, were extracted from the normalized one-dimensional correlation function ($\gamma(r)$) following the method of Vonk and Goderis as described in the experimental part [49–51]. Representative examples of $\gamma(r)$ for T_c of 111 and 114 °C are given in Fig. 10(a) and (b) respectively for the indicated values of t_c (additional plots for other values of T_c are provided in Figure SI5). The linear regression of the autocorrelation triangle (shown as diagonal red dashed lines in Fig. 10) was used to calculate the linear crystallinity (φ), which was further used to estimate the value of the flat region of the first

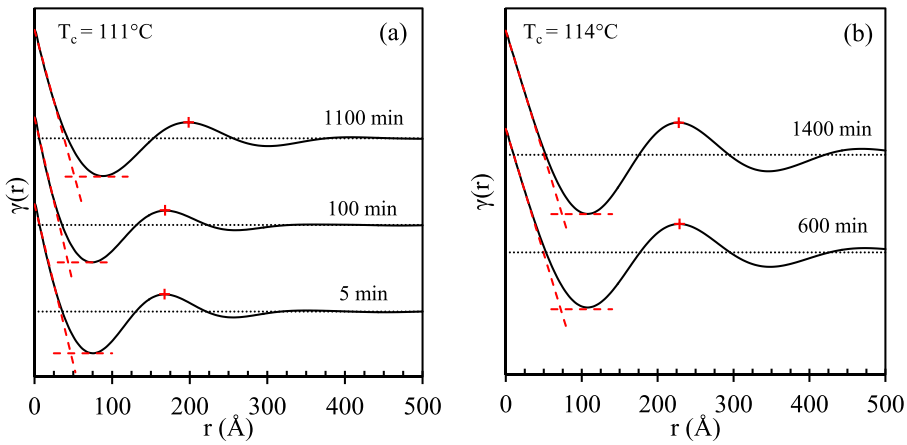

Fig. 10. Normalized one-dimensional correlation function $\gamma(r)$ for T_c of (a) 111 °C and (b) 114 °C for the indicated values of t_c. The correlation triangle and flat region of the first minimum are shown as dashed red lines while the first maximum (long spacing) is indicated by red plus signs. The plots have been vertically shifted for clarity. (For interpretation of the references to colour in this figure legend, the reader is referred to the Web version of this article.)

Table 1
Structural information from the normalized one-dimensional correlation function.($\gamma(r)$)

T_c (°C)	t_c (min)	L (Å)	l_a (Å)	l_c (Å)	# Ester Layers
111	5	168	47	121	2.53
111	100	168	43	125	2.60
111	1100	199	52	147	3.06
112	30	166	46	120	2.54
112	60	165	45	120	2.55
112	300	165	44	121	2.56
112	800	176	40	136	2.86
112	1200	184	38	146	3.06
113	600	172	46	126	2.67
113	2000	200	46	154	3.20
113	3000	214	53	153	3.17
114	600	229	73	156	3.21
114	1400	227	74	153	3.15
114.5	600	226	67	159	3.28
114.5	1400	222	74	148	3.06
115	2000	222	63	159	3.27

minimum (shown as horizontal, red dashed lines). Values of φ are listed in Table SI3 and compared with the value of X_c (calculated using Equation (1)). As expected, φ is slightly greater than X_c. The flat region of the first minimum was typically very close to the actual first minimum of $\gamma(r)$ as can be seen in Fig. 10. L was obtained as the first maximum of $\gamma(r)$ and has values very close to those found directly from the Lorentz-corrected SAXS patterns, as shown in Table SI3. As discussed in the experimental part, the thickness at the flat region of the first minimum of $\gamma(r)$ corresponds to the shortest correlation distance, and thus depends on the level of crystallinity. For the PE-48,48 samples analyzed, the level of crystallinity is >65%, therefore the distance determined from $\gamma(r)$ as $\varphi \times L$ corresponds to l_a, and l_c is $L - l_a$. The calculated values of L, l_a, and l_c are listed in Table 1. For $T_c \leq 113$ °C, l_c increases from 120 to 150 Å as t_c increases, while above the transition for $T_c > 113$ °C, l_c is high and remains basically constant at ~155 ± 4 Å. A representative example of the variation of L, l_a, and l_c with time is depicted in Fig. 11(a) for $T_c = 112$ °C. As shown, the temporal increase in l_c largely scales with the increase in L.

From the l_c data and the observed layer periodicity (d), the average number of ester layers normal to the basal surface of the lamellae can be computed. Whether the number of layers is an integer or non-integer value is important to test the proposed correlation between the discrete increase in melting and the completion of an integer number of ester layers during isothermal crystallization. The data are listed in the last column of Table 1 and are plotted in Fig. 11(b). The squares are data below the transition ($T_c \leq 113$ °C) for which both LT and HT crystals are present. The circles are data for $T_c \geq 114$ °C at which only HT crystals are formed. An arrow has been drawn to indicate the increase of l_c with increasing time for $T_c \leq 113$ °C.

For $T_c \leq 113$ °C at relatively short t_c, the computed number of layers is ~2.5 and increases to 3 at the longest t_c when the level of isothermal thickening is very high. Conversely, for $T_c \geq 114$ °C, the number of layers is basically 3 and is unchanged with t_c. These data support the schematic model for isothermal thickening of PE-48,48 shown in Fig. 12. Under isothermal crystallization conditions, for $T_c \leq 113$ °C lamellar crystals with a non-integer number of ester layers (~2.5) develop first. For these lamellae, the order emanating from the crystals is dissipated at a distance relatively far from the ester moiety, along the methylene sequence. Because the basal lamellar surface of these crystals does not require a specific staggering of the ester groups, the structure with a non-integer number of layers is the kinetically favored lamellar structure. However, the thicker structure with an integer number of layers is a thermodynamically more stable structure. Therefore, with time, the non-integer structure that develops first evolves to the one with the integer number of layers, as shown in the schematics.

Thickening to a structure that staggers the ester groups at the surface, thus minimizing the basal surface free energy (σ_e) compared to the surface of the non-integer structure, explains the observed discrete melting behavior. While methylene units are added to the *all-trans* orthorhombic symmetry during isothermal thickening of the non-integer structure, the topology of the interface remains basically unchanged, resulting in a continuous, relatively small increase in melting, as shown by the ~1.5 °C increase of the LT peak in Fig. 6(a) and (b). It is only when the accretion of methylene units from the interface to the crystal reaches the ester group that the topology of the lamellae surface changes drastically. Such change in σ_e will cause the step increase in melting even with a relatively small change in crystal thickness.

An estimate of the change in σ_e that will correspond to the observed ~5 °C change in melting temperature can be acquired using the

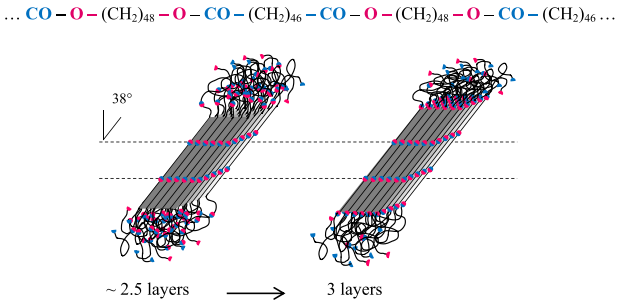

Fig. 12. Proposed model of isothermal step thickening observed in PE-48,48. Time increases from left to right as the crystalline structure evolves to have an integer (3) number of ester layers.

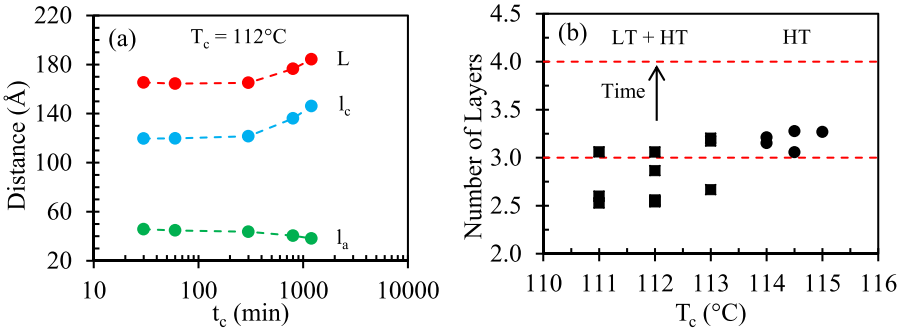

Fig. 11. (a) Long period (L), crystal thickness (l_c), and amorphous thickness (l_a) as a function of t_c for T_c of 112 °C. (b) The estimated number of layers calculated as l_c/d plotted vs. T_c. For $T_c \leq 113$ °C (LT + HT), data are shown as squares, while for $T_c \geq 114$ °C (HT), data are shown as circles. An arrow has been drawn to indicate crystal thickening with increasing time for $T_c \leq 113$ °C.

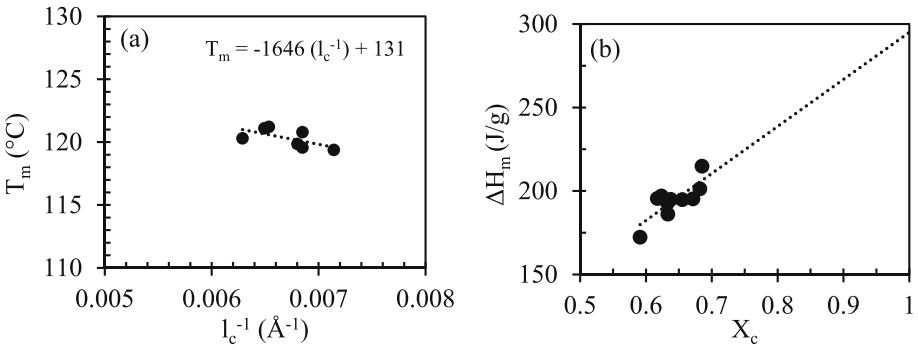

Fig. 13. (a) Gibbs-Thomson plot for HT crystals of PE-48,48 and (b) extrapolation of the observed heat of fusion as a function of the WAXD crystallinity (X_c) to 100% crystallinity.

simplified Gibbs-Thompson equation for lamellae crystals [60], given as,

$$T_m = T_m^\circ \left[1 - \frac{2\sigma_e}{l_c \Delta H_u}\right] \quad (6)$$

First, using the highest observed melting temperatures after isothermal crystallization at the longest t_c, and the corresponding l_c values obtained from SAXS, a T_m° of 131 ± 4 °C was obtained (Fig. 13(a)). The heat of fusion of the pure crystal, $\Delta H_u = 2.98 \times 10^9$ erg/cm^3, was obtained by extrapolating the observed heat of fusion and the corresponding WAXD crystallinity to 100% crystallinity (Fig. 13(b)). With T_m° and ΔH_u values, from the slope of Fig. 13(a), a value of $\sigma_e = 61 \pm 1$ erg/cm^2 is obtained for the integer layered crystallites. With this σ_e value as reference, we find that σ_e needs to be increased about 20% to account for the 30 Å difference in crystal thickness and the ~5 °C difference in melting between HT and LT crystallites.

Explicitly, for the LT crystals of PE-48,48, taking average values of l_c and σ_e of 122 Å and 75 erg/cm^2, and for the HT crystals 153 Å and 65 erg/cm^2 respectively, the calculated values of T_m from Equation (6) are 114.4 °C and 119.5 °C, which match very closely the observed melting endotherms of Fig. 6. These data support the model for isothermal thickening of Fig. 12 driven by minimizing surface energy by chain extension in the *c* axis up to completion of the ester layer and placement of the ester moiety at the lamellar basal surface.

Whether thickening is favored by straightening the PE-48,48 sequences flanked by the alkoxy units [-O–CH_2–$(CH_2)_{46}$–CH_2–O-] due perhaps to a more favored staggering at the surface, as shown in the schematics, rather than by straightening the carboxyl-flanked sequences, is an open question that could be further addressed with well-oriented WAXD fiber patterns. These details are beyond the scope of the present study.

4. Conclusions

The long-spaced aliphatic polyester PE-48,48 undergoes the usual slow thickening observed in other semi-crystalline polymers, as well as a unique isothermal step thickening leading to a discrete increase in melting temperature with increasing crystallization time. The latter is associated with layered lamellar crystals that, during isothermal crystallization, undergo thickening and reach a thickness that corresponds to an integer number of ester layers. It is perceived that staggering the ester moieties at the lamellar surface lowers the surface free energy of the lamellae crystals, thus increasing their thermal stability.

Analogous isothermal step thickening has been seen previously in long-chain *n*-alkanes and low molecular weight PEO fractions. In these monodisperse, low molar mass systems, discontinuous thickening is driven by the thermodynamic need to pair chain ends at the basal lamellae surfaces, an effect which is absent in polydisperse, high molar mass polymers. The results presented herein for PE-48,48 represent the first known instance of isothermal step thickening with a discrete increase in melting behavior observed in high molecular weight polymers.

The isothermal increase in lamellae thickness and discrete increase in melting temperatures of PE-48,48 is observed at $T_c \leq 113$ °C for which the thickness of the initial crystals is between 2 and 3 ester layers. Completion of the layer during thickening increases symmetry of the lamellar stack, and stabilizes the crystals compared to those with a non-integer layer thickness. For $T_c > 113$ °C, the initial crystal thickness is at or very close to the full 3 layers. The more stable crystals do not undergo further step thickening.

The isothermal thickening process follows logarithmic time dependence, as shown for the increase of crystal thickness of linear polyethylene [1] and is thermally activated with the same activation energy of 238 ± 4 kJ/mol found for the re-folding of low molar mass fractions of polyethylene oxide [27].

Declaration of competing interest

The authors declare that they have no known competing financial interests or personal relationships that could have appeared to influence the work reported in this paper.

CRediT authorship contribution statement

Stephanie F. Marxsen: Resources, Data curation, Formal analysis, Writing - original draft, Writing - review & editing. **Manuel Häußler:** Resources. **Stefan Mecking:** Resources. **Rufina G. Alamo:** Conceptualization, Project administration, Resources, Supervision, Formal analysis, Writing - original draft, Writing - review & editing, Funding acquisition.

Acknowledgements

Funding of this work by the National Science Foundation, Polymer Program DMR 1607786, is gratefully acknowledged. We are indebted to the High Performance Materials Institute of Florida State University for access to X-ray instrumentation. M.H. and S.M. acknowledge financial support by the Baden-Württemberg Foundation.

Appendix A. Supplementary data

Supplementary data to this article can be found online at https://doi.org/10.1016/j.polymer.2020.122282.

References

[1] T. Albrecht, G. Strobl, Observation of the early stages of crystallization in polyethylene by time-dependent SAXS: transition from individual crystals to stacks of lamellae, Macromolecules 29 (1996) 783–785, https://doi.org/10.1021/ma9503524.

[2] J. Dlugosz, G.V. Fraser, D. Grubb, A. Keller, J.A. Odell, P.L. Goggin, Study of crystallization and isothermal thickening in polyethylene using SAXD, low frequency Raman spectroscopy and electron microscopy, Polymer 17 (1976) 471–480, https://doi.org/10.1016/0032-3861(76)90125-7.

[3] P.J. Barham, A. Keller, The initial stages of crystallization of polyethylene from the melt, J. Polym. Sci., Part B: Polym. Phys. 27 (1989) 1029–1042, https://doi.org/10.1002/polb.1989.090270506.

[4] G.M. Stack, L. Mandelkern, I.G. Voigt-Martin, Changes in crystallite size distribution during the isothermal crystallization of linear polyethylene, Polym. Bull. 8 (1982) 421–428, https://doi.org/10.1007/BF00265262.

[5] M.J. McCready, J.M. Schultz, J.S. Lin, R.W. Hendricks, Effect of crystallization time on the properties of melt-crystallized linear polyethylene, J. Polym. Sci. Polym. Phys. Ed 17 (1979) 725–740, https://doi.org/10.1002/pol.1979.180170501.

[6] J.D. Hoffman, J.J. Weeks, Melting process and the equilibrium melting temperature of polychlorotrifluoroethylene, J. Res. Natl. Bur. Stand. Sect. A Phys. Chem. 66A (1962) 13, https://doi.org/10.6028/jres.066A.003.

[7] J.D. Hoffman, J.J. Weeks, X-Ray study of isothermal thickening of lamellae in bulk polyethylene at the crystallization temperature, J. Chem. Phys. 42 (1965) 4301–4302, https://doi.org/10.1063/1.1695935.

[8] R.A. Chivers, P.J. Barham, J. Martinez-Salazar, A. Keller, A new look at the crystallization of polyethylene. II. Crystallization from the melt at low supercoolings, J. Polym. Sci. Polym. Phys. Ed 20 (1982) 1717–1732, https://doi.org/10.1002/pol.1982.180200921.

[9] D.C. Bassett, A.M. Hodge, R.H. Olley, On the morphology of melt-crystallized polyethylene II. Lamellae and their crystallization conditions, Proc. R. Soc. A Math. Phys. Eng. Sci. 377 (1981) 39–60, https://doi.org/10.1098/rspa.1981.0114.

[10] I.G. Voigt-Martin, L. Mandelkern, A quantitative electron-microscopic study of a linear polyethylene fraction crystallized at different temperatures, J. Polym. Sci. Polym. Phys. Ed 19 (1981) 1769–1790, https://doi.org/10.1002/pol.1981.180191109.

[11] P. Dreyfus, A. Keller, A simple chain refolding scheme for the annealing behavior of polymer crystals, J. Polym. Sci. B Polym. Lett. 8 (1970) 253–258, https://doi.org/10.1002/pol.1970.110080407.

[12] P. Dreyfuss, A. Keller, Chain folding in polyamides: a study on Nylons 66, 610, and 612 as crystallized from solution, J. Macromol. Sci. Part B. 4 (1970) 811–835, https://doi.org/10.1080/00222347008217125.

[13] P.J. Phillips, G.J. Rensch, Crystallization studies of poly(ϵ-caprolactone). II. Lamellar thickening and melting, J. Polym. Sci., Part B: Polym. Phys. 27 (1989) 155–173, https://doi.org/10.1002/polb.1989.090270110.

[14] R.G. Alamo, K.W. McLaughlin, L. Mandelkern, Changes in the phase structure of the polyethylenes after long-time storage at room temperatures, Polym. Bull. 22 (1989) 299–306, https://doi.org/10.1007/BF00282856.

[15] R.G. Alamo, L. Mandelkern, G.M. Stack, C. Kroehnke, G. Wegner, Isothermal thickening of crystals of high-molecular-weight n-alkanes, Macromolecules 26 (1993) 2743–2753, https://doi.org/10.1021/ma00063a017.

[16] A. Kawaguchi, T. Ichida, S. Murakami, K. Katayama, Thickening process of polyethylene single crystals at an early stage of annealing, Colloid Polym. Sci. 262 (1984) 597–604, https://doi.org/10.1007/BF01452449.

[17] T. Ichida, M. Tsuji, S. Murakami, A. Kawaguchi, K. Katayama, Thickening process of polyethylene single crystals at an early stage of annealing - II. Computer simulation of lamellar thickening, Colloid Polym. Sci. 263 (1985) 293–300, https://doi.org/10.1007/BF01412244.

[18] J. Hobbs, M. Hill, P. Barham, Crystallization and isothermal thickening of single crystals of C246H494 in dilute solution, Polymer 42 (2001) 2167–2176, https://doi.org/10.1016/S0032-3861(00)00450-X.

[19] G. Ungar, A. Keller, Time-resolved synchrotron X-ray study of chain-folded crystallization of long paraffins, Polymer 27 (1986) 1835–1844, https://doi.org/10.1016/0032-3861(86)90169-2.

[20] S.J. Organ, A. Keller, The onset of chain folding in ultralong n-alkanes: an electron microscopic study of solution-grown crystals, J. Polym. Sci., Part B: Polym. Phys. 25 (1987) 2409–2430, https://doi.org/10.1002/polb.1987.090251201.

[21] G. Ungar, S.J. Organ, Isothermal refolding in crystals of long alkanes in solution. I. Effect of surface 'self-poisoning, J. Polym. Sci., Part B: Polym. Phys. 28 (1990) 2353–2363, https://doi.org/10.1002/polb.1990.090281213.

[22] G. Ungar, X.B. Zeng, S.J. Spells, Non-integer and mixed integer forms in long n -alkanes observed by real-time LAM spectroscopy and SAXS, Polymer 41 (2000) 8775–8780, https://doi.org/10.1016/S0032-3861(00)00220-2.

[23] R.G. Alamo, The crystallization behavior of long chain N-alkanes and low molecular weight polyethylenes, in: M. Dosiere (Ed.), Crystallization of Polymers; Advanced Study Institute NATO Series C, Klumer Academic Pub, Boston, 1993, pp. 73–79.

[24] S.N. Magonov, N.A. Yerina, G. Ungar, D.H. Reneker, D.A. Ivanov, Chain unfolding in single crystals of ultralong alkane C 390 H 782 and polyethylene: an atomic force microscopy study, Macromolecules 36 (2003) 5637–5649, https://doi.org/10.1021/ma0301303.

[25] X.-M. Zhai, W. Wang, Z.-P. Ma, X.-J. Wen, F. Yuan, X.-F. Tang, B.-L. He, Spontaneous and inductive thickenings of lamellar crystal monolayers of low molecular weight PEO fractions on surface of solid substrates, Macromolecules 38 (2005) 1717–1722, https://doi.org/10.1021/ma047764+.

[26] S.J. Organ, G. Ungar, A. Keller, Isothermal refolding in crystals of long alkanes in solution. II. Morphological changes accompanying thickening, J. Polym. Sci., Part B: Polym. Phys. 28 (1990) 2365–2384, https://doi.org/10.1002/polb.1990.090281214.

[27] X.-F. Tang, X.-J. Wen, X.-M. Zhai, N. Xia, W. Wang, G. Wegner, Z.-H. Wu, Thickening process and kinetics of lamellar crystals of a low molecular weight poly (ethylene oxide), Macromolecules 40 (2007) 4386–4388, https://doi.org/10.1021/ma070414d.

[28] P.J.P. Arlie, P. Spegt, A. Skoulios, Etude de la cristallisation des polymères. II. Structure lamellaire et repliement des chaînes du polyoxyéthylène, Makromol. Chem. 104 (1967) 212–229, https://doi.org/10.1002/macp.1967.021040122.

[29] P.P.A. Spegt, J. Terrisse, B. Gilg, A. Skoulios, Étude de la cristallisation des polyèmres. III. Détermination de la température de fusion et cinétique de fusion isotherme des polyoxyéthylènes de faible masse moléculaire, Makromol. Chem. 107 (1967) 29–38, https://doi.org/10.1002/macp.1967.021070103.

[30] A.J. Kovacs, A. Gonthier, Crystallization and fusion of self-seeded polymers, Kolloid-Z. Z. Polym. 250 (1972) 530–552, https://doi.org/10.1007/BF01507524.

[31] A.J. Kovacs, A. Gonthier, C. Straupe, Isothermal growth, thickening, and melting of poly(ethylene oxide) single crystals in the bulk, J. Polym. Sci., Polym. Symp. 50 (1975) 283–325, https://doi.org/10.1002/polc.5070500117.

[32] A.J. Kovacs, C. Straupe, A. Gonthier, Isothermal growth, thickening, and melting of polyethylene oxide) single crystals in the bulk. II, J. Polym. Sci., Polym. Symp. 59 (1977) 31–54, https://doi.org/10.1002/polc.5070590105.

[33] S.Z.D. Cheng, A. Zhang, J.S. Barley, J. Chen, A. Habenschuss, P.R. Zschack, Isothermal thickening and thinning processes in low-molecular-weight poly (ethylene oxide) fractions. 1. From nonintegral-folding to integral-folding chain crystal transitions, Macromolecules 24 (1991) 3937–3944, https://doi.org/10.1021/ma00013a030.

[34] S.Z.D. Cheng, J. Chen, A. Zhang, J.S. Barley, A. Habenschuss, P.R. Zschack, Isothermal thickening and thinning processes in low molecular weight poly (ethylene oxide) fractions crystallized from the melt: 2. Crystals involving more than one fold, Polymer 33 (1992) 1140–1149, https://doi.org/10.1016/0032-3861(92)90757-N.

[35] A.J. Kovacs, C. Straupe, Isothermal growth, thickening and melting of poly (ethylene-oxide) single crystals in the bulk. III. Bilayer crystals and the effect of chain ends, J. Cryst. Growth 48 (1980) 210–226, https://doi.org/10.1016/0022-0248(80)90211-0.

[36] S.Z.D. Cheng, A. Zhang, J. Chen, D.P. Heberer, Nonintegral and integral folding crystal growth in low-molecular mass poly(ethylene oxide) fractions. I. Isothermal lamellar thickening and thinning, J. Polym. Sci., Part B: Polym. Phys. 29 (1991) 287–297, https://doi.org/10.1002/polb.1991.090290304.

[37] S.Z.D. Cheng, J. Chen, A. Zhang, D.P. Heberer, Nonintegral and integral folding crystal growth in low-molecular mass poly (ethylene oxide) fractions. II. End-group effect: α,ω-methoxy-poly (ethylene oxide), J. Polym. Sci., Part B: Polym. Phys. 29 (1991) 299–310, https://doi.org/10.1002/polb.1991.090290305.

[38] K. Song, S. Krimm, Raman longitudinal acoustic mode (LAM) studies of folded-chain morphology in poly(ethylene oxide) (PEO). 3. Chain folding in PEO as a function of molecular weight, Macromolecules 23 (1990) 1946–1957, https://doi.org/10.1021/ma00209a012.

[39] X. Zhang, X. Zuo, P. Ortmann, S. Mecking, R.G. Alamo, Crystallization of long-spaced precision polyacetals I: melting and recrystallization of rapidly formed crystallites, Macromolecules 52 (2019) 4934–4948, https://doi.org/10.1021/acs.macromol.9b00922.

[40] P. Kaner, C. Ruiz-Orta, E. Boz, K.B. Wagener, M. Tasaki, K. Tashiro, R.G. Alamo, Kinetic control of chlorine packing in crystals of a precisely substituted polyethylene. Toward advanced polyolefin materials, Macromolecules 47 (2014) 236–245, https://doi.org/10.1021/ma401541r.

[41] X. Zhang, L. Santonja-Blasco, K.B. Wagener, E. Boz, M. Tasaki, K. Tashiro, R. G. Alamo, Infrared spectroscopy and X-ray diffraction characterization of dimorphic crystalline structures of polyethylenes with halogens placed at equal distance along the backbone, J. Phys. Chem. B 121 (2017) 10166–10179, https://doi.org/10.1021/acs.jpcb.7b08877.

[42] T.W. Gaines, E.B. Trigg, K.I. Winey, K.B. Wagener, High melting precision sulfone polyethylenes synthesized by ADMET chemistry, Macromol. Chem. Phys. 217 (2016) 2351–2359, https://doi.org/10.1002/macp.201600118.

[43] S. Reimann, V. Danke, M. Beiner, W.H. Binder, Synthesis of supramolecular precision polymers: crystallization under conformational constraints, J. Polym. Sci. Part A Polym. Chem. 55 (2017) 3736–3748, https://doi.org/10.1002/pola.28759.

[44] L.R. Middleton, S. Szewczyk, J. Azoulay, D. Murtagh, G. Rojas, K.B. Wagener, J. Cordaro, K.I. Winey, Hierarchical acrylic acid aggregate morphologies produce strain-hardening in precise polyethylene-based copolymers, Macromolecules 48 (2015) 3713–3724, https://doi.org/10.1021/acs.macromol.5b00797.

[45] K.J. Arrington, C.B. Murray, E.C. Smith, H. Marand, J.B. Matson, Precision polyketones by ring-opening metathesis polymerization: effects of regular and irregular ketone spacing, Macromolecules 49 (2016) 3655–3662, https://doi.org/10.1021/acs.macromol.6b00590.

[46] E.B. Trigg, B.J. Tiegs, G.W. Coates, K.I. Winey, High morphological order in a nearly precise acid-containing polymer and ionomer, ACS Macro Lett. 6 (2017) 947–951, https://doi.org/10.1021/acsmacrolett.7b00450.

[47] V. Danke, G. Gupta, S. Reimann, W.H. Binder, M. Beiner, Structure formation in nanophase-separated systems with lamellar morphology: comb-like vs. linear precision polymers, Eur. Polym. J. 103 (2018) 116–123, https://doi.org/10.1016/j.eurpolymj.2018.03.041.

[48] T. Witt, M. Häußler, S. Kulpa, S. Mecking, Chain multiplication of fatty acids to precise telechelic polyethylene, Angew. Chem. Int. Ed. 56 (2017) 7589–7594, https://doi.org/10.1002/anie.201702796.

[49] C.G. Vonk, A.P. Pijpers, An x-ray diffraction study of nonlinear polyethylene. I. Room-temperature observations, J. Polym. Sci. Polym. Phys. Ed 23 (1985) 2517–2537, https://doi.org/10.1002/pol.1985.180231210.

[50] C.G. Vonk, G. Kortleve, X-ray small-angle scattering of bulk polyethylene, Kolloid-Z. Z. Polym. 220 (1967) 19–24, https://doi.org/10.1007/BF02086052.

[51] B. Goderis, H. Reynaers, M.H.J. Koch, V.B.F. Mathot, Use of SAXS and linear correlation functions for the determination of the crystallinity and morphology of semi-crystalline polymers. Application to linear polyethylene, J. Polym. Sci., Part B: Polym. Phys. 37 (1999) 1715–1738, https://doi.org/10.1002/(SICI)1099-0488(19990715)37:14<1715::AID-POLB15>3.0.CO;2-F.

[52] Z. Denchev, A. Nogales, T.A. Ezquerra, J. Fernandes-Nascimento, F.J. Balta-Calleja, On the origin of the multiple melting behavior in poly(ethylene naphthalene-2,6-dicarboxylate): microstructural study as revealed by differential scanning calorimetry and X-ray scattering, J. Polym. Sci., Part B: Polym. Phys. 38 (2000) 1167–1182, https://doi.org/10.1002/(SICI)1099-0488(20000501)38:9<1167::AID-POLB8>3.0.CO;2-8.

[53] C. Santa Cruz, N. Stribeck, H.G. Zachmann, F.J. Balta Calleja, Novel aspects in the structure of poly(ethylene terephthalate) as revealed by means of small angle x-ray scattering, Macromolecules 24 (1991) 5980–5990, https://doi.org/10.1021/ma00022a013.

[54] X. Zhang, W. Zhang, K.B. Wagener, E. Boz, R.G. Alamo, Effect of self-poisoning on crystallization kinetics of dimorphic precision polyethylenes with bromine, Macromolecules 51 (2018) 1386–1397, https://doi.org/10.1021/acs.macromol.7b02745.

[55] A. Almontassir, S. Gestí, L. Franco, J. Puiggalí, Molecular packing of polyesters derived from 1,4-butanediol and even aliphatic dicarboxylic acids, Macromolecules 37 (2004) 5300–5309, https://doi.org/10.1021/ma049939l.

[56] T. Kanamoto, K. Tanaka, H. Nagai, Growth and morphology of single crystals of linear aliphatic polyesters, J. Polym. Sci. 2 Polym. Phys. 9 (1971) 2043–2060, https://doi.org/10.1002/pol.1971.160091109.

[57] G. Ungar, X. Zeng, Learning polymer crystallization with the aid of linear, branched and cyclic model compounds, Chem. Rev. 101 (2001) 4157–4188, https://doi.org/10.1021/cr990130u.

[58] K.J. Fritzsching, K. Mao, K. Schmidt-Rohr, Avoidance of density anomalies as a structural principle for semicrystalline polymers: the importance of chain ends and chain tilt, Macromolecules 50 (2017) 1521–1540, https://doi.org/10.1021/acs.macromol.6b02000.

[59] D.S.M. de Silva, X. Zeng, G. Ungar, S.J. Spells, Chain tilt and surface disorder in lamellar crystals. A FTIR and SAXS study of labeled long alkanes, Macromolecules 35 (2002) 7730–7741, https://doi.org/10.1021/ma0206669.

[60] R.G. Alamo, L. Mandelkern, Thermodynamic quantities governing melting, in: J. Mark (Ed.), Physical Properties of Polymers Handbook, Springer-Verlag, New York, 2007, pp. 165–186.